Exact Bit Error-Rate Analysis of Two-User NOMA Using QAM With Arbitrary Modulation Orders

Tasneem Assaf, *Member, IEEE*, Arafat J. Al-Dweik, *Senior Member, IEEE*, Mohamed S. El Moursi, *Senior Member, IEEE*, Hatem Zeineldin, *Senior Member, IEEE*, and Mohammad Al-Jarrah, *Member, IEEE*

***Abstract*— This letter considers the exact bit error rate (BER) analysis of a two-user non-orthogonal multiple access (NOMA) system using square quadrature amplitude modulation (QAM). Unlike existing work, no constraints are imposed on the modulation order of the QAM symbols for any user. Closed-form expressions are derived for the BER of the successive interference cancellation (SIC) receiver in Raleigh fading channels. The analytical BER results corroborated by Mote Carlo simulation show that the power control becomes challenging for high order QAM. Moreover, the BER of each user is approximately independent of the modulation scheme used by the other user for certain power settings.**

***Index Terms*— Non-orthogonal multiple access (NOMA), bit error rate (BER), joint detection, multiuser detection, successive interference cancellation (SIC), quadrature amplitude modulation (QAM).**

I. Introduction

NON-ORTHOGONAL multiple access (NOMA) is an efficient multiple access technique, which is considered as a promising candidate for future wireless communication networks. Although NOMA has received an increased attention recently, it is based on well-known schemes such as superposition coding and successive interference cancellation (SIC) [1]. NOMA can improve the spectral efficiency by allowing multiple users to share the transmission resources simultaneously, at the expense of some additional receiver complexity and bit error rate (BER) degradation [2]. Several NOMA schemes have been proposed in the literature, but the main categories are the code-domain [3], [4] and power-domain NOMA [5], [6], which is the focus of this work. In the literature, SIC has been widely considered as the main detection scheme for power-domain NOMA [4], [7]–[14]. However, SIC detectors (SICDs) suffer from long processing times because the nth user has to sequentially detect and subtract the signals of all users whose indices are less than n [15]. To reduce the processing time, joint multiuser detector (JMuD) has been proposed as an alternative for the SICD [15]–[18].

The BER analysis of downlink NOMA using SICDs has received extensive attention in the recent literature. For example, the pairwise error probability is derived in [12], [19] using quadrature phase shift keying (QPSK), and it is used to compute a union bound on the BER. However, the union bound can be far from the exact BER for several operating conditions as shown in [7]. The exact BER for NOMA over Nakagami-m channels is derived in [7] for two and three-user scenarios using QPSK. In [20], the BER performance for three-user NOMA using SICD is investigated where space shift keying (SSK) is considered. The BER analysis is also considered in [21] for cooperative NOMA where the BER for the signals in the first phase is evaluated by an approximation. In the second phase, the relay uses SSK to send the signal to the far user. Therefore, the exact BER analysis for the first and second users using QAM is not considered. In [9], the BER is investigated for NOMA using SICDs under Rayleigh fading channels where exact and approximate closed-form expressions are derived for downlink and uplink, respectively. The presented expressions are applicable for the two-user NOMA using only binary phase shift keying (BPSK) and QPSK. In [22], the BER for downlink NOMA is derived for any number of users using BPSK. Exact symbol error rate (SER) analysis for NOMA using quadrature amplitude modulation (QAM) is presented in [23], [24]. Although SER is a useful indicator for the system error performance, the BER is more informative and it is the standard metric for error rate performance.

As can be noted from the aforementioned discussion, the surveyed literature, and to the best of the authors' knowledge, there is no work that considers the exact BER analysis of NOMA using QAM with arbitrary modulation orders, which is the main objective of this work.

The rest of the letter is organized as follows. In Sec. II, the system and channel models are presented. The exact BER analysis for the first and second users are presented in Sec. III and IV, respectively. Numerical and simulation results are given in Sec. V. Finally, the work is concluded in Sec. VI.

Manuscript received August 21, 2020; accepted August 24, 2020. Date of publication August 28, 2020; date of current version December 10, 2020. This work was supported by Khalifa University under the flagship project entitled "MUSES: Multiuse Space Energy Systems" under Grant 8474000026. The work of Arafat J. Al-Dweik was supported by the KU Center for Cyber-Physical Systems, under Grant C2PS-T2. The associate editor coordinating the review of this letter and approving it for publication was Y. Liu. *(Corresponding author: Arafat J. Al-Dweik.)*

Tasneem Assaf and Mohamed S. El Moursi are with the Department of Electrical Engineering and Computer Science, Khalifa University, Abu Dhabi, United Arab Emirates (e-mail: tasneem.assaf@ku.ac.ae; mohamed.elmoursi@ku.ac.ae).

Arafat J. Al-Dweik is with the Department of Electrical Engineering and Computer Science, Khalifa University, Abu Dhabi, United Arab Emirates, also with the Center for Cyber Physical Systems (C2PS), Khalifa University, Abu Dhabi, United Arab Emirates, and also with the Department of Electrical and Computer Engineering, Western University, London, ON N6A 3K7, Canada (e-mail: dweik@fulbrightmail.org).

Hatem Zeineldin is with the Faculty of Engineering, Cairo University, Giza 12613, Egypt, on leave from the Department of Electrical Engineering and Computer Science, Khalifa University, Abu Dhabi, United Arab Emirates (e-mail: hatem.zeineldin@ku.ac.ae).

Mohammad Al-Jarrah is with the School of Electrical and Electronic Engineering, The University of Manchester, Manchester M13 9PL, U.K. (e-mail: mohammad.al-jarrah@manchester.ac.uk).

Digital Object Identifier 10.1109/LCOMM.2020.3020161

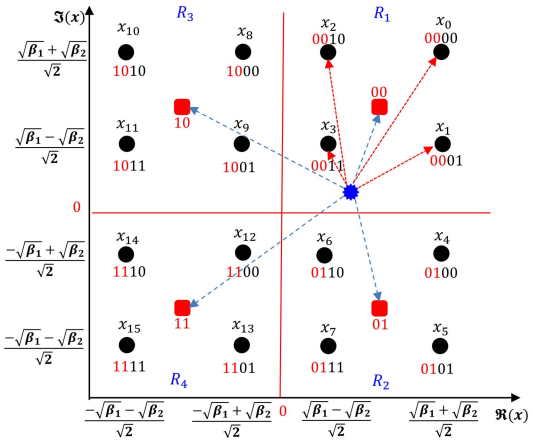

Fig. 1. The constellation diagram of the transmitted NOMA symbol x.

II. System Model

This work considers a downlink power-domain NOMA system that supports two simultaneous users, U_1 and U_2. All users equipment (UE) and the base station (BS) are equipped with a single antenna [7], and the data for U_1 and U_2 are modulated using square QAM with modulation orders M_1 and M_2. Gray coding is used to map the bits of each user before being multiplexed to form the NOMA symbol. The inphase and quadrature components of a QAM symbol are respectively given by

$$A_{n_I} = \pm (2k_n - 1), \quad k_n \in \{1, 3, \ldots, \Lambda_n\} \tag{1}$$

$$A_{n_q} = \pm (2l_n - 1), \quad l_n \in \{1, 3, \ldots, \Lambda_n\}. \tag{2}$$

Given that all symbols are equally probable with unity minimum Euclidean distance (ED), the average energy for the nth user can be expressed as $E_n = \frac{2}{3}(M_n - 1)$. Therefore, the QAM symbol of the nth user $s_n = A_{n_I} + jA_{n_q}$, $j = \sqrt{-1}$, $s_n \in \mathbb{S}_n = \{d_0, d_1, \ldots, d_{M_n - 1}\}$. Therefore, the NOMA signal transmitted from the BS can be described as

$$x = \sqrt{\frac{\beta_1 P_T}{E_1}} s_1 + \sqrt{\frac{\beta_2 P_T}{E_2}} s_2 \tag{3}$$

where s_n is selected uniformly from the nth QAM constellation with modulation order M_n, P_T is the BS total transmit power, which is normalized to unity, and β_n is the power allocation coefficient for the nth user, $\beta_1 + \beta_2 = 1$. Consequently, $\mathbb{E}\left[|x|^2\right] = 1$, where $\mathbb{E}[\cdot]$ denotes the statistical average. An example for the resultant NOMA constellation for $M_1 = M_2 = 4$ is shown in Fig. 1. In the figure, the first user bits are the leftmost two bits and the second user bits are the rightmost two bits. The NOMA symbol x has a 16-point constellation.

In flat fading channels, the received signal at the nth UE can be expressed as [4]

$$r_n = h_n x + w_n \tag{4}$$

where $h_n = \sqrt{q_n^{-\zeta}}\hbar_n$, q_n is the distance between the BS and nth user, ζ is the path-loss exponent, $\hbar_n \sim \mathcal{CN}(0, 1)$ is the small-scale channel fading parameter, and $w_n \sim \mathcal{CN}(0, N_0)$ is the additive white Gaussian noise (AWGN). Given that the channel phase $\arg\{h_n\} \triangleq \theta_n$ is estimated and compensated perfectly at the receiver, then the received signal after phase compensation $\check{r}_n = r_n e^{-j\theta_n} = \alpha_n x + \check{w}_n$, where

TABLE I
Notations Used Throughout the Letter

$B_n = \log_2 M_n$	$L_{1,n} = (1 - 2^{-i})\sqrt{M_n} - 1$
$\Lambda_n = \sqrt{M_n} - 1$	$M = M_1 \times M_2$
$v_n = \log_2 \sqrt{M_n}$	$\varphi_1 = \frac{1}{\sqrt{2}}\left(\sqrt{\beta_1} + \sqrt{\beta_2}\right)$
$\lambda_{i,k,n} = \left\lfloor \frac{k2^{i-1}}{\sqrt{M_n}} \right\rfloor$	$\varphi_2 = \frac{1}{\sqrt{2}}\left(\sqrt{\beta_1} - \sqrt{\beta_2}\right)$
$\epsilon_n = \frac{\alpha_n}{\sigma_{n_n}}$	$g_n^{\pm}(a, b) = \epsilon_n \sqrt{q_n^{-\zeta}}\left(a\sqrt{\frac{\beta_1}{E_1}} \pm b\sqrt{\frac{\beta_2}{E_2}}\right)$
$Q(g_1(a, b)) = Q\left(g_1^+(a, b)\right) - Q\left(g_1^-(a, b)\right)$	

TABLE II
The Ratio of β_1/β_2 for Various Values of M_1 and M_2

M_1, M_2	$4, 16$	$16, 4$	$4, 64$	$64, 4$	$16, 64$	$64, 16$
β_1/β_2	1.8	5	7/3	21	35/3	37.8

$\check{w}_n = w_n e^{-j\theta_n}$ and $\alpha_n = |h_n|$ is the channel envelope which follows Rayleigh distribution. Assuming that the AWGN is circularly symmetric, then $\check{w}_n$ and w_n have identical probability density functions (PDFs), consequently $\check{w}_n$ and w_n can be used interchangeably. Without loss of generality, it is assumed that the first user has the lowest channel gain, and the second user has the second lowest channel gain, and so forth, i.e., $\alpha_1 < \alpha_2$. To enable reliable detection of all users, it is necessary to cancel the inter-user interference (IUI), which is typically performed using SIC. Therefore, the power should be allocated in the opposite order of the channel gains, i.e., $\beta_1 > \beta_2$ [7], [12]. Moreover, for proper implementation and avoiding overlap between the users' symbols, the power allocation coefficients must satisfy the following range constraint [24],

$$\frac{\beta_1}{\beta_2} > \frac{M_1 - 1}{M_2 - 1}\Lambda_2^2. \tag{5}$$

For $M_1 = M_2$ we obtain $\beta_1/\beta_2 > \Lambda_2^2$, where Λ_2 and all other notations used throughout the letter are shown in Table I. The ratio for different values of M_1 and M_2 is shown in Table II. To extract the information symbols s_n $\forall n$, the SICD can be used as described in Sec. III and IV for U_1 and U_2, respectively.

III. BER Analysis of U_1

The SICD for U_1 is similar to the single user maximum likelihood detector (MLD) used with QAM signals. Therefore,

$$\hat{s}_1 = \arg\min_{s_1 \in \mathbb{S}_1} \left| r_1 - \hat{h}_1 \sqrt{\frac{\beta_1}{E_1}} s_1 \right|^2 \tag{6}$$

where $\hat{h}_1$ is the estimated value of h_1. In this work we assume perfect channel estimation, thus $\hat{h}_1 = h_1$. Based on the constellation in Fig. 1, it can be noted that U_1 bits in each of the four quadrants $\{R_0, R_1, R_2, R_3\}$ are fixed regardless of U_2 bits. Therefore, computing and comparing the EDs with any four symmetrical points would result in the same decision when the ED with the 16 constellation points is computed. For example, the constellation points that correspond to x_0, x_5, x_{10} and x_{15} in Fig. 1 are symmetrical and they can be used to detect $\hat{s}_1$. Or equivalently, we can use M_1 virtual constellation points obtained from the scaled set $\sqrt{\frac{\beta_i}{E_i}}\mathbb{S}_1$, which are marked using the solid squares in Fig. 1.

TABLE III

REGULAR PATTERNS FOR $C(b_{1i})$, $F_1(b_{1i})$, AND $F_2(b_{1i})$ FOR THE BER OF THE FIRST USER

$C\left(b_{11}\right)$	1	..	..	..	1	1	..	..	1	..	1	..	1
$F_1\left(b_{11}\right)$	1	..	..	..	1	3	..	..	3	..	Λ_1	..	Λ_1
$F_2\left(b_{11}\right)$	1	-1	..	..	$\mp\Lambda_2$	1	..	..	$\mp\Lambda_2$	..	1	..	$\mp\Lambda_2$
$C\left(b_{12}\right)$	2	..	..	..	2	1	..	..	1	..	-1	..	-1
$F_1\left(b_{12}\right)$	1	..	..	..	1	3	..	..	3	..	$\frac{3}{2}\sqrt{M_1}-1$	..	$\frac{3}{2}\sqrt{M_1}-1$
$F_2\left(b_{12}\right)$	1	-1	..	..	$\mp\Lambda_2$	1	-1	..	$\mp\Lambda_2$	..	1	..	$\mp\Lambda_2$
...	...												
$C\left(b_{1v_1}\right)$	$\frac{1}{2}\sqrt{M_1}$	..	..	..	$\frac{1}{2}\sqrt{M_1}-1$	$\frac{1}{2}\sqrt{M_1}-1$			$\frac{1}{2}\sqrt{M_1}-1$	..	-1		-1
$F_1\left(b_{1v_1}\right)$	1	..	..	..	1	3	..	..	3	..	$2\sqrt{M_1}-3$	..	$2\sqrt{M_1}-3$
$F_2\left(b_{1v_1}\right)$	1	-1	..	..	$\mp\Lambda_2$	1	-1	..	$\mp\Lambda_2$	..	1	..	$\mp\Lambda_2$

The bit representation for each point in the NOMA constellation diagram can be expressed as b_{ni}, where the user index $n \in \{1,2\}$ and the bit index $i \in \{1,2,\ldots,B_n\}$, where the first leftmost B_1 bits belong to U_1. To simplify the presentation, we initially consider the case of $M_1 = M_2 = 4$ shown in Fig. 1, and then the approach is generalized for an arbitrary M_1 and M_2. For this scenario, each NOMA symbol consists of 4 bits, 2 bits from each user. For b_{11}, the constellation can be divided into two regions based on the decision boundary, which is the y-axis. In this case, the decision boundary and the constellation point can be at a distance of φ_1 or φ_2, and the error event for b_{11} depends on the transmitted NOMA symbol. For example, if x_0, x_1, x_4 or x_5 is transmitted, then $\Pr\left(\hat{b}_{11} \neq b_{11}\right) = \Pr(\mathfrak{n}_1 < -\alpha_1\varphi_1)$, $\mathfrak{n}_1 \triangleq \Re\left(\breve{w}_1\right)$, and similarly, if x_2, x_3, x_6 or x_7 is transmitted, then $\Pr\left(\hat{b}_{11} \neq b_{11}\right) = \Pr(\mathfrak{n}_1 < -\alpha_1\varphi_2)$. The case for b_{12} is similar to b_{11}, except that the decision boundary is the x-axis, consequently, $P_{b_{11}} = P_{b_{12}}$. By considering all cases and the fact that $P_{b_{11}} = P_{b_{12}}$, the average conditional BER for U_1 can be expressed as

$$\begin{aligned} P_{U_1} &= \frac{1}{2}\sum_{i=0}^{2} P_{b_{1i}} \\ &= \frac{1}{2}\left[Q\left(\epsilon_1\varphi_1\right) + Q\left(\epsilon_1\varphi_2\right)\right] \end{aligned} \tag{7}$$

where $Q(\cdot)$ is the Q-function and $\sigma^2_{\mathfrak{n}_1} = N_0/2$.

Applying the same approach for various values of M_1 and M_2 indicates that the errors' events follow a specific pattern, which allows using induction to derive the BER for an arbitrary M_n. One of the main observations is that the error probabilities of the $B_n/2$ leftmost and rightmost bits are identical, and hence, only one of them should be derived. Moreover, for an arbitrary M_n, $P_{b_{1i}}$ has the following general expression

$$P_{b_{1i}} = \sum_{l}\sum_{k} C\left(b_{1i}\right) Q\left(g_1^{+}\left(F_1\left(b_{1i}\right), F_2\left(b_{1i}\right)\right)\right). \tag{8}$$

For b_{11}, $C\left(b_{11}\right) = 1$, and it is repeated $2B_2$ times. For b_{1v_1}, the value of $C\left(b_{1v_1}\right)$ starts with $\sqrt{M_1}/2$, which is repeated Λ_2 times. The $\left(\sqrt{M_2}+1\right)$th value of $C\left(b_{1v_1}\right)$ is the first value decreased by 1 and repeated Λ_2 times. The $\left(3\sqrt{M_2}\right)$th value is the $\left(\sqrt{M_2}+1\right)$th term with a different sign and repeated Λ_2 times. This pattern repeats for the remaining terms until the value of $C\left(b_{1v_1}\right)$ becomes -1, and repeated Λ_2. The other patterns for $C\left(b_{1i}\right)$ are presented in Table III. For $F_1\left(b_{1i}\right)$, it starts at 1 and ends at $2\left\lceil\left(1-2^i\right)\sqrt{M_1}-1\right\rceil+1$ where each term is repeated $\sqrt{M_2}$ times as shown in Table III. Similarly, the $F_2\left(b_{1i}\right)$ patterns can be obtained from Table III. As example for using Table III is shown in Table IV for $M_1 = M_2 = 16$.

TABLE IV

PARAMETERS EVALUATION FOR $M_1 = M_2 = 16$, $\bar{1} \triangleq -1$ AND $\bar{3} \triangleq -3$

$C\left(b_{11}\right)$	1	1	1	1								
$F_1\left(b_{11}\right)$	1	1	1	1	3	3	3	3				
$F_2\left(b_{11}\right)$	1	$\bar{1}$	3	$\bar{3}$	1	$\bar{1}$	3	$\bar{3}$				
$C\left(b_{12}\right)$	2	2	2	2	1	1	1	1	$\bar{1}$	$\bar{1}$	$\bar{1}$	$\bar{1}$
$F_1\left(b_{12}\right)$	1	1	1	1	3	3	3	3	5	5	5	5
$F_2\left(b_{12}\right)$	1	$\bar{1}$	3	$\bar{3}$	1	$\bar{1}$	3	$\bar{3}$	1	$\bar{1}$	3	$\bar{3}$

From the regularities shown in Table III, the probability that the bit b_{1i} is in error can be formulated as follows:

$$P_{b_{1i}} = \frac{1}{\sqrt{M}}\sum_{k=0}^{L_{1,1}}\sum_{l=0}^{\Lambda_2} D_1\left(i,k\right) Q\left(g_1^{+}\left(2k+1, 2l-\sqrt{M_2}+1\right)\right) \tag{9}$$

where

$$D_1\left(i,k\right) = (-1)^{\lambda_{i,k,1}}\left(2^{i-1} - \left\lfloor\frac{k2^{i-1}}{\sqrt{M_1}} + \frac{1}{2}\right\rfloor\right).$$

As can be noted from (9), $P_{b_{1i}}$ is conditioned on the instantaneous signal-to-noise ratio (SNR), which is defined as

$$\left[g_1^{+}\left(2k+1, 2l-\sqrt{M_2}+1\right)\right]^2 \triangleq \gamma_1. \tag{10}$$

Therefore, the unconditional bit error can be obtained as

$$\bar{P}_{b_{1i}} = \int_0^{\infty} P_{b_{1i}}\ f\left(\gamma_1\right) d\gamma_1 \tag{11}$$

where the PDF of γ_1 is given by

$$f\left(\gamma_1\right) = \frac{1}{\bar{\gamma}_1}\exp\left(-\frac{\gamma_1}{\bar{\gamma}_1}\right) \tag{12}$$

in (12), $\bar{\gamma}_1 = \mathbb{E}\left(\gamma_1\right)$. By substituting (9) and (12) into (11) we obtain

$$\bar{P}_{b_{1i}} = \frac{1}{\sqrt{M}}\sum_{k=0}^{L_{1,1}}\sum_{l=0}^{\Lambda_2} D_1\left(i,k\right)\left[1-\sqrt{\frac{\bar{\gamma}_1}{\bar{\gamma}_1+2}}\right]. \tag{13}$$

And finally, the average unconditional BER can be computed as

$$\bar{P}_{U_1} = \frac{2}{v_1}\sum_{i=1}^{v_1}\bar{P}_{b_{1i}}. \tag{14}$$

IV. BER Analysis of U_2

For U_2 symbols, the SIC detector can be described as,

$$\hat{s}_2 = \arg\min_{s_2 \in \mathbb{S}_2} \left| r_n - \hat{h}_2 \sqrt{\frac{\beta_1}{E_1}} \hat{s}_1 - \hat{h}_2 \sqrt{\frac{\beta_2}{E_2}} s_2 \right|^2 \quad (15)$$

where $\hat{s}_1$ is the estimated U_1 symbols and $\hat{h}_2$ is the estimated value of h_2. Therefore, the probability of error for U_2 depends on $\hat{s}_1$, which is obtained in the first stage of the SIC process described in Sec. III. More specifically, Fig. 1 shows that the error event for a particular bit for U_2 depends only on b_{11} in $\hat{s}_1$. For example, given that x_0 is transmitted, then b_{21} will be detected incorrectly if x_0 is detected as one of the symbols in the second column of the constellation diagram, i.e., $\{x_2, x_3, x_6, x_7\}$, or if it is detected as one of the symbols in the fourth column $\{x_{10}, x_{11}, x_{14}, x_{15}\}$, which corresponds to the case where $\Re\{r_2\}$ is in the intervals $\left[\alpha_2\sqrt{\frac{\beta_1}{2}}, 0\right]$ or $\left[-\alpha_2\sqrt{\frac{\beta_1}{2}}, -\infty\right]$. The same observation can be made for b_{22} except that the bit will be detected incorrectly if x_0 is detected as any of the symbols in the second $\{x_1, x_3, x_9, x_{11}\}$ or fourth $\{x_5, x_7, x_{13}, x_{15}\}$ rows, and the error depends only on b_{12} in $\hat{s}_1$. Consequently, the bit error will occur if $\Im\{r_2\}$ is in the intervals $\left[\alpha_2\sqrt{\frac{\beta_1}{2}}, 0\right]$ or $\left[-\alpha_2\sqrt{\frac{\beta_1}{2}}, -\infty\right]$. As a result, the error events for b_{21} and b_{22} will have the same probability. For higher M_1 and M_2 values, the same approach can used except that the bits of each user will be divided into two equal groups each of which has v_2 bits, and the two groups will have the same BER. The error events and probability of error for each bit in each group should be computed following the same approach used for the $M_1 = M_2 = 4$ example. After an exhaustive study of several modulation orders, it was interestingly found that the bits' errors for U_2 bits have a fixed pattern that can be used to derive a general expression for the BER, which is given by

$$P_{b_{2i}} = \frac{1}{\sqrt{M}} \sum_{k=0}^{L_{1,2}} \sum_{l=0}^{2\Lambda_1} S D_2(i,k) D_3(i,l) Q\left(g_2^+(c_i l, 2k+1)\right) - \sum_{k=0}^{L_{1,2}} \sum_{l=1}^{2\Lambda_1} S D_2(i,k) D_3(i,l) Q\left(g_2^-(c_i l, 2k+1)\right) \quad (16)$$

where

$$S = (-1)^{\left\lfloor \frac{l 2^{v_2}+i-1}{\sqrt{M_2}} \right\rfloor + \lambda_{i,k,2}}, \quad c_i = 2 - \delta_{i,1}$$
$$D_2(i,k) = 2^{i-1} - \left\lfloor \frac{k 2^{i-1}}{\sqrt{M_2}} + \frac{1}{2} \right\rfloor$$
$$D_3(i,l) = 2^{v_1} - \left\lfloor \frac{l}{2^{1-(i-1)\log_2\left(\sqrt{M_1}-1\right)}} + \frac{1}{2} \right\rfloor. \quad (17)$$

Moreover, the simplified BER formulae for several values of M_1 and M_2 are given in [25]. Similar to U_1 case, the unconditional $P_{b_{2i}}$ over Rayleigh fading channels can be obtained as

$$\bar{P}_{b_{2i}} = \int_0^\infty P_{b_{2i}}^+ f\left(\gamma_2^+\right) d\gamma_2^+ + \int_0^\infty P_{b_{2i}}^- f\left(\gamma_2^-\right) d\gamma_2^- \quad (18)$$

where $P_{b_{2i}}^+$ and $P_{b_{2i}}^-$ are the first and second parts of $P_{b_{2i}}$ (16), $\gamma_2^\pm \triangleq \left[g_2^\pm(c_i l, 2k+1)\right]^2$ and $\bar{\gamma}_2^\pm = \mathbb{E}\left(\gamma_2^\pm\right)$ are the instantaneous and average SNRs, respectively, the PDF of $\gamma_2^\pm$ is similar to (12). By substituting (16) and the PDFs of γ_2^+ and γ_2^- into (18) and evaluating the integrals we obtain

$$\bar{P}_{b_{2i}} = \sum_{k=0}^{L_{1,2}} \sum_{l=0}^{2\Lambda_1} \frac{P_C^+}{\sqrt{M}} S D_2(i,k) D_3(i,l) Q\left(g_2^+(c_i l, 2k+1)\right) - \sum_{k=0}^{L_{1,2}} \sum_{l=1}^{2\Lambda_1} \frac{P_C^-}{\sqrt{M}} S D_2(i,k) D_3(i,l) \times Q\left(g_2^-(c_i l, 2k+1)\right) \Bigg). \quad (19)$$

where $P_C^\pm = \left[1 - \sqrt{\frac{\bar{\gamma}_2^\pm}{\bar{\gamma}_2^\pm + 2}}\right]$. Finally, the average BER can be expressed as

$$\bar{P}_{U_2} = \frac{2}{v_2} \sum_{i=1}^{v_2} \bar{P}_{b_{2i}}. \quad (20)$$

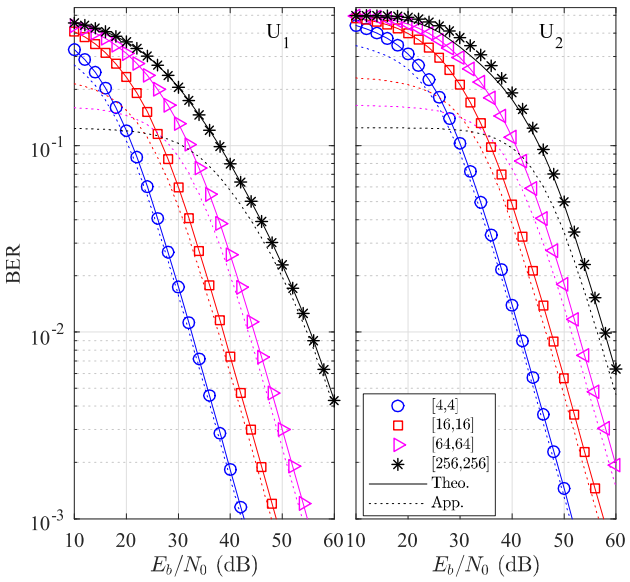

Fig. 2. Average BER using various modulation orders for U_1 and U_2 where $M_1 = M_2$.

V. Numerical and Simulation Results

This section presents the analytical and Monte Carlo simulation results where $q_1 = 6.015$, $q_2 = 1$, $\zeta = 2$. The power allocation factors β_n are selected to satisfy (5) where $M_1 = M_2 = 256$, more specifically, $\beta_1 = 0.99657$, and $E_b/N_0 = 1/\sigma_{\mathbf{n}_1}^2 = 1/\sigma_{\mathbf{n}_2}^2$. In the legends of the presented figures, the modulation orders are arranged as $[M_1, M_2]$.

Fig. 2 shows the analytical and simulated BER of U_1 and U_2 for various modulation orders where $M_1 = M_2$. As can be noted, the analytical and simulation results match very well for all the considered values of M_1, M_2, and SNR. Moreover, the figure shows the trade-off between the power assignment and BER for each user. For example, because $\beta_1 \gg \beta_2$ in the case of QPSK, the BER for U_1 will be much lower than U_2 because β_1 is much larger than the threshold (5) required to prevent the constellations overlap. In particular for the considered system, U_1 requires 11 dB less than U_2 to obtain BER of 10^{-3}. For the case of $M_1 = M_2 = 256$, β_1 value is very close to the threshold, therefore, the performance is mostly determined by the channel conditions, and U_1 needs roughly an additional 2 dB as compared to U_2 to obtain BER

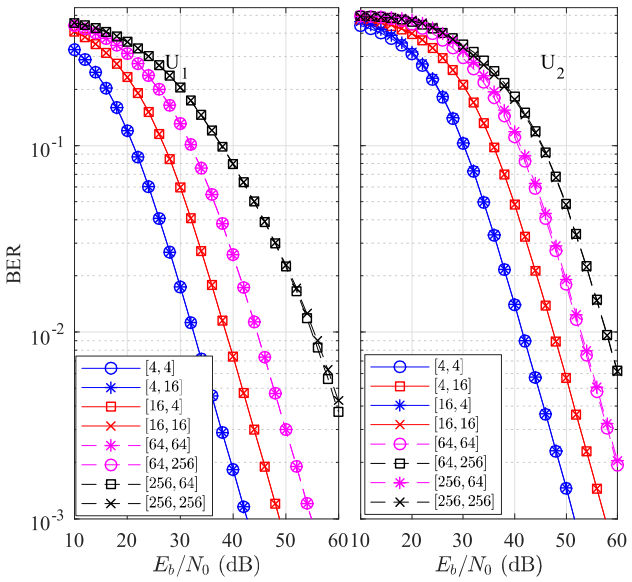

Fig. 3. Average BER using various modulation orders for U_1 and U_2 using various values of M_1 and M_2.

of 10^{-3}. It is worth noting that the power allocation will be challenging for high modulation orders as the value of β_2 will be extremely small, which is hard to tune. Fig. 2 also shows the BER calculated using the typical approximation, dividing SER by $\log_2(M)$ [23], [24], where it is shown that the approximation is close only for low order modulation such as QPSK, or for high SNRs, otherwise, the approximation error is substantial.

Fig. 3 shows the BER for U_1 and U_2 where the modulation order for one user is fixed while varying the modulation order for the other. Interestingly, it can be noted that changing the modulation order of one user has nearly a negligible effect on the BER of the other user for such power settings. For example, the BERs of U_1 for the cases of $[4, 4]$ and $[4, 16]$ are identical. The same conclusion applies to the cases of $\{[16, 16], [16, 64]\}$ and $\{[64, 64], [64, 256]\}$. Nevertheless, a slight discrepancy at high SNRs is observed for the case of $\{[256, 64], [256, 256]\}$. The same trends can be noted for U_2.

VI. Conclusion

This work derived the exact BER expressions in closed-form for a two-user NOMA system using square QAM with arbitrary modulation order. The BER analysis was carried out using the SIC detector. The presented numerical examples showed that the difference between β_1 and β_2 can be substantial for high modulation orders. For example, using $M_1 = M_2 = 64$ implies that $\beta_1 > 49\beta_2$. Therefore, the power assignment becomes a critical matter as inaccurate assignment may cause interference. Moreover, for certain power values, it is shown that the BER for each user is nearly invariant when the modulation order of the other user is varied.

References

[1] R. Zhang and L. Hanzo, "A unified treatment of superposition coding aided communications: Theory and practice," *IEEE Commun. Surveys Tuts.*, vol. 13, no. 3, pp. 503–520, 3rd Quart., 2011.

[2] L. Dai, B. Wang, Z. Ding, Z. Wang, S. Chen, and L. Hanzo, "A survey of non-orthogonal multiple access for 5G," *IEEE Commun. Surveys Tuts.*, vol. 20, no. 3, pp. 2294–2323, 3rd Quart., 2018.

[3] M. Al-Imari, M. A. Imran, R. Tafazolli, and D. Chen, "Subcarrier and power allocation for LDS-OFDM system," in *Proc. IEEE 73rd Veh. Technol. Conf. (VTC Spring)*, May 2011, pp. 1–5.

[4] F. Kara and H. Kaya, "On the error performance of cooperative-NOMA with statistical CSIT," *IEEE Commun. Lett.*, vol. 23, no. 1, pp. 128–131, Jan. 2019.

[5] S. M. R. Islam, N. Avazov, O. A. Dobre, and K.-S. Kwak, "Power-domain non-orthogonal multiple access (NOMA) in 5G systems: Potentials and challenges," *IEEE Commun. Surveys Tuts.*, vol. 19, no. 2, pp. 721–742, 2nd Quart., 2017.

[6] J. Ding, J. Cai, and C. Yi, "An improved coalition game approach for MIMO-NOMA clustering integrating beamforming and power allocation," *IEEE Trans. Veh. Technol.*, vol. 68, no. 2, pp. 1672–1687, Feb. 2019.

[7] T. Assaf, A. Al-Dweik, M. E. Moursi, and H. Zeineldin, "Exact BER performance analysis for downlink NOMA systems over Nakagami-m fading channels," *IEEE Access*, vol. 7, pp. 134539–134555, Sep. 2019.

[8] Q. He, Y. Hu, and A. Schmeink, "Closed-form symbol error rate expressions for non-orthogonal multiple access systems," *IEEE Trans. Veh. Technol.*, vol. 68, no. 7, pp. 6775–6789, Jul. 2019.

[9] F. Kara and H. Kaya, "BER performances of downlink and uplink NOMA in the presence of SIC errors over fading channels," *IET Commun.*, vol. 12, no. 15, pp. 1834–1844, Sep. 2018.

[10] M. Zeng, A. Yadav, O. A. Dobre, G. I. Tsiropoulos, and H. V. Poor, "Capacity comparison between MIMO-NOMA and MIMO-OMA with multiple users in a cluster," *IEEE J. Sel. Areas Commun.*, vol. 35, no. 10, pp. 2413–2424, Oct. 2017.

[11] S. K. Zaidi, S. F. Hasan, and X. Gui, "Evaluating the ergodic rate in SWIPT-aided hybrid NOMA," *IEEE Commun. Lett.*, vol. 22, no. 9, pp. 1870–1873, Sep. 2018.

[12] L. Bariah, S. Muhaidat, and A. Al-Dweik, "Error probability analysis of non-orthogonal multiple access over nakagami-m fading channels," *IEEE Trans. Commun.*, vol. 67, no. 2, pp. 1586–1599, Feb. 2019.

[13] T. Hou, Y. Liu, Z. Song, X. Sun, and Y. Chen, "Multiple antenna aided NOMA in UAV networks: A stochastic geometry approach," *IEEE Trans. Commun.*, vol. 67, no. 2, pp. 1031–1044, Feb. 2019.

[14] X. Li, Q. Wang, Y. Liu, T. A. Tsiftsis, Z. Ding, and A. Nallanathan, "UAV-aided multi-way NOMA networks with residual hardware impairments," *IEEE Wireless Commun. Lett.*, early access, May 22, 2020, doi: 10.1109/LWC.2020.2996782.

[15] B. K. Ng and C.-T. Lam, "Joint power and modulation optimization in two-user non-orthogonal multiple access channels: A minimum error probability approach," *IEEE Trans. Veh. Technol.*, vol. 67, no. 11, pp. 10693–10703, Nov. 2018.

[16] C. Yan, A. Harada, A. Benjebbour, Y. Lan, A. Li, and H. Jiang, "Receiver design for downlink non-orthogonal multiple access (NOMA)," in *Proc. IEEE 81st Veh. Technol. Conf. (VTC Spring)*, May 2015, pp. 1–6.

[17] M. Qiu, Y.-C. Huang, S.-L. Shieh, and J. Yuan, "A lattice-partition framework of downlink non-orthogonal multiple access without SIC," *IEEE Trans. Commun.*, vol. 66, no. 6, pp. 2532–2546, Jun. 2018.

[18] S.-L. Shieh, C.-H. Lin, Y.-C. Huang, and C.-L. Wang, "On gray labeling for downlink non-orthogonal multiple access without SIC," *IEEE Commun. Lett.*, vol. 20, no. 9, pp. 1721–1724, Sep. 2016.

[19] L. Bariah, S. Muhaidat, and A. Al-Dweik, "Error performance of NOMA-based cognitive radio networks with partial relay selection and interference power constraints," *IEEE Trans. Commun.*, vol. 68, no. 2, pp. 765–777, Feb. 2020.

[20] F. Kara and H. Kaya, "Performance analysis of SSK-NOMA," *IEEE Trans. Veh. Technol.*, vol. 68, no. 7, pp. 6231–6242, Jul. 2019.

[21] Q. Li, M. Wen, E. Basar, H. V. Poor, and F. Chen, "Spatial modulation-aided cooperative NOMA: Performance analysis and comparative study," *IEEE J. Sel. Topics Signal Process.*, vol. 13, no. 3, pp. 715–728, Jun. 2019.

[22] M. Aldababsa, C. Goztepe, G. K. Kurt, and O. Kucur, "Bit error rate for NOMA network," *IEEE Commun. Lett.*, vol. 24, no. 6, pp. 1188–1191, Jun. 2020.

[23] E. M. Almohimmah and M. T. Alresheedi, "Error analysis of NOMA-based VLC systems with higher order modulation schemes," *IEEE Access*, vol. 8, pp. 2792–2803, 2020.

[24] I. Lee and J. Kim, "Average symbol error rate analysis for non-orthogonal multiple access with M-Ary QAM signals in rayleigh fading channels," *IEEE Commun. Lett.*, vol. 23, no. 8, pp. 1328–1331, Jun. 2019.

[25] T. Assaf, A. Al-Dweik, M. E. Moursi, and H. Zeineldin, "Exact bit error-rate analysis of two-user NOMA using QAM with arbitrary modulation orders," *IEEE TechRxiv*, May 2020, doi: 10.36227/techrxiv.12310169.v1.